Secreted Msn Phosphorylated by PKM2 Function in the Tumor Micro-Environment

Amir Hamza , Oyungerel Dogsom , Shohel Mahmud , Jae-Bong Park *

Posted Date: 26 February 2026

doi: 10.20944/preprints202602.1249.v1

Keywords: extracellular moesin; extracellular PKM2; tumor microenvironment; p-Thr413 moesin

 doi:10.20944/preprints202602.1249.v1

Article

Secreted Msn Phosphorylated by PKM2 Function in the Tumor Micro-Environment

Amir Hamza [1,2], Oyungerel Dogsom [1,2,3], Shohel Mahmud [1,4] and Jae-Bong Park [1,2,5,*]

[1] Department of Biochemistry, Hallym University College of Medicine, Chuncheon, Kangwon-do 24252, Republic of Korea
[2] Institute of Cell Differentiation and Aging, Hallym University College of Medicine, Chuncheon, Kangwon-do 24252, Republic of Korea
[3] Department of Biology, School of Bio-Medicine, Mongolian National University of Medical Sciences, Ulaanbaatar 14210, Mongolia
[4] National Institute of Biotechnology, Ganakbari, Ashulia, Savar 1349, Dhaka, Bangladesh
[5] ELMED Co., 218, Bio Building 1, 32 Soyanggang-gil, Chuncheon, Gangwon-do 24232, Republic of Korea
* Correspondence: jbpark@hallym.ac.kr; Tel.: 82-33-248-2542; Fax, 82-33-244-8425

Abstract

Tumor-secreted proteins represent valuable molecular targets for cancer diagnosis and therapy. Moesin (Msn) has been reported to be secreted into the tumor microenvironment (TME) and to promote malignant progression; however, its extracellular regulatory mechanisms remain poorly understood. In this study, we identified extracellular moesin (exMsn) as a common secretory protein derived from 4T1 breast cancer cells and RAW264.7 macrophages using mass spectrometry, which was further validated by western blotting. Functional analyses demonstrated that exMsn enhanced cancer cell migration through activation of the RhoA/ROCK and ZEB1 signaling axes. Neutralization of exMsn using a specific antibody significantly reduced reactive oxygen species production and cell migration. We further observed that extracellular pyruvate kinase M2 (exPKM2) phosphorylated extracellular proteins in the TME, among which exMsn was identified by peptide mass fingerprinting (PMF) and confirmed by in vitro kinase assays. Mechanistically, exPKM2 phosphorylated exMsn in a phosphoenolpyruvate (PEP)-dependent manner, and site-directed mutagenesis revealed Thr413 as the primary phosphorylation site. This phosphorylation may protect exMsn from extracellular degradation. Additionally, exPKM2 physically interacted with exMsn, with this interaction enhanced during cancer–macrophage co-culture. Collectively, our findings un-cover a novel extracellular exPKM2–exMsn signaling mechanism that promotes tumor progression and may provide new therapeutic targets.

Keywords: extracellular moesin; extracellular PKM2; tumor microenvironment; p-Thr413 moesin

1. Introduction

Tumor cells secrete various extracellular molecules that communicate with near-by stromal cells within the tumor microenvironment (TME) [1]. These secretory mediators consist of cytokines, chemokines, glycolytic enzymes and other factors, which modify the characteristics of cancer and play crucial roles in tumor development, thereby serving as tumor biomarkers or therapeutic targets [2–4]. Some extracellular proteins, like pyruvate kinase M2 (PKM2) [5], matrix metalloproteinases (MMPs) [6], and Hsp90α [7] have been identified as key promoters of cell migration, invasion and angiogenesis within the TME. Despite recent discoveries expanding our understanding of proteins linked to tumors, the specific interaction networks and molecular mechanisms through which extracellular proteins influence tumor progression remains un-clear.

ERM proteins, part of the FERM 4.1 protein superfamily, include Ezrin, Radixin, and Moesin (Msn) (ERM), displaying significant structural and functional similarities across various species [8,9].

 doi:10.20944/preprints202602.1249.v1

These proteins act as pivotal connectors, linking actin filaments to the plasma membrane, facilitating crucial cellular functions such as adhesion, microvilli formation, motility, and signal transduction [10–12]. The phosphorylation of specific threonine residues (T567 in ezrin, T564 in radixin, and T558 in Msn) triggers ERM protein activation, unveiling binding sites for interaction with other molecules [13,14]. Among these proteins, Msn assumes particular significance in endothelial cells, playing a fundamental role in angiogenesis [15]; therefore, alterations in Msn functionality could potentially influence this process [16,17].

However, Msn also plays a significant role in the context of cancer [17,18]. It is involved in various aspects of cancer development and progression, making it a compelling subject for research in the field of oncology. Notably, the ERM family proteins are recognized for their significant involvement in numerous essential physiological and pathological processes, encompassing cell polarity, division, metastasis, as well as the creation of protrusions and the immunological synapse [7,19]. With its role in maintaining cell shape, facilitating cell-cell communication, and modulating mem-brane-cytoskeleton interactions. Thus, Msn has emerged as a focal point for extensive biochemical research.

Msn has classically been characterized as an intracellular protein; how-ever, accumulating evidence indicates that Msn also exhibits extracellular localization and functional activity in specific pathological contexts [20]. A recent report indicates that extracellular Msn differentially regulates breast cancer cell behavior by modulating Src signaling and promoting the nuclear translocation of β-catenin [21]. Msn per-forms distinct functions depending on its subcellular localization, acting within the cytosol and nucleus or in the extracellular space. For example, pyruvate kinase M2 (PKM2) is predominantly localized intracellularly, where it functions not only as a glycolytic enzyme catalyzing the conversion of phosphoenolpyruvate (PEP) to pyruvate, but also as a protein kinase and transcriptional regulator [22–25]. However, the secreted form of (PKM2 is abundantly detected in lung cancer, where it functions as an autocrine signaling molecule that transcriptionally activates MMP9, thereby promoting metastatic progression [26]. Additionally, PKM2 has been reported to be secreted via exosomes from hepatocellular carcinoma (HCC) cells, where it promotes the differentiation of monocytes into macrophages [27]. In our previous study, we demonstrated that PKM2 is secreted by macrophages and functions as a paracrine signaling molecule that promotes cancer cell migration by the induction of p-Tyr42 RhoA and epithelial-mesenchymal transition (EMT) marker genes [5]. Among the secreted proteins, heat shock protein 90 (HSP90) stabilizes proteins under intra-cellular condition [28], while it acts as a pro-tumorigenic protein under extracellular condition [29,30]. A recent report showed that, extracellular HSP90α supports the extracellular PKM2 and promotes tumor metastasis through the GRP78-AKT signaling axis [30]. Thus, we hypothesized that, extracellular Msn may have a role in cancer progression, when it is associated with extracellular PKM2 in the TME.

In this study, we identify Msn as a common secretory molecule derived from both cancer cells and macrophages. We demonstrate that Msn physically interacts with pyruvate kinase M2 (PKM2) in both the cytosol and the extracellular tumor microenvironment. Moreover, we establish that PKM2 phosphorylates Msn at the Thr413 residue. Although the functional role of phosphorylated Msn in cancer requires further investigation, our findings suggest that Msn contributes to cancer progression and may represent a potential therapeutic target.

2. Results

2.1. Msn Was Identified as Being Secreted from Cancer (4T1) and Macrophage (Raw264.7) Cells

In our previous study, conditioned media (CM) from RAW264.7 macrophages induced superoxide generation, proliferation, and migration in 4T1 breast cancer cells, while CM from 4T1 cells increased superoxide production, migration, and differentiation of RAW264.7 macrophages, including polarization toward M1 and M2 phenotypes [5]. These results indicate reciprocal functional interactions mediated by secreted factors between macrophages and cancer cells. Moreover, secreted

 doi:10.20944/preprints202602.1249.v1

factors from both macro-phages and cancer cells exhibited reciprocal activity within the tumor microenvironment. To identify shared secretory proteins, concentrated conditioned media were separated by SDS-PAGE and analyzed by MALDI-TOF mass spectrometry, which identified Msn as a common secreted molecule from both 4T1 cancer cells and RAW264.7 macrophages (Figure 1A; Figure S1a). To further confirm the secretion of candidate proteins, western blot analysis was performed on cytosolic and secreted fractions. PKM2 was predominantly secreted by RAW264.7 macrophages, cathepsin L (CTSL) was mainly secreted by 4T1 cancer cells, and Msn was detected as a common secretory protein in both cell types (Figure 1B and C). The three-dimensional (3D) crystal structure of Msn is available in the Protein Data Bank (PDB ID: 2I1J) [31] (Figure 1D) and corresponds to a 68-kDa ERM (Ezrin-Redixin-Moesin) family protein involved in actin cytoskeleton dynamics [32]. However, the extracellular Msn function remains unclear. Thus we hypothesized that Msn acts as a ligand protein or an effector protein in the TME. To perform further functional analyses, we prepared Msn recombinant protein. GST-Msn plasmid (Addgene, plasmid #11637) was expressed in E. coli, and the recombinant GST-Msn fusion protein was purified. Following thrombin cleavage, recombinant moesin (rMsn) was obtained, and protein purity was confirmed by SDS-PAGE alongside 1 μg of rGST-PKM2 as a positive control (Figure 1E). Moreover, the relative secretion amount of Msn was confirmed by western blot analysis in which an identical amount of cancer and macrophage cells were used. Western blot analysis revealed that Msn was secreted from both cells approximately ~400 ng in 20 μg/well loaded CM compared to the positive control of rGST-Msn (Figure 1F). Among more than 20 secreted proteins identified from both cell types, Msn was consistently detected as one of the most abundant extracellular molecules. Kaplan–Meier analysis using the KM plotter database showed that high intracellular Msn mRNA expression was associated with poor overall survival in gastric cancer patients, although it was not statistically significant (Figure 1G). Based on this association, Msn was selected for subsequent functional analyses as it could be a critical candidate for cancer treatment. Collectively, these results show that Msn is a shared and quantitatively abundant extracellular protein secreted by both macrophages and breast cancer cells and emerges as a compelling candidate mediator of tumor–immune cell crosstalk in the tumor microenvironment.

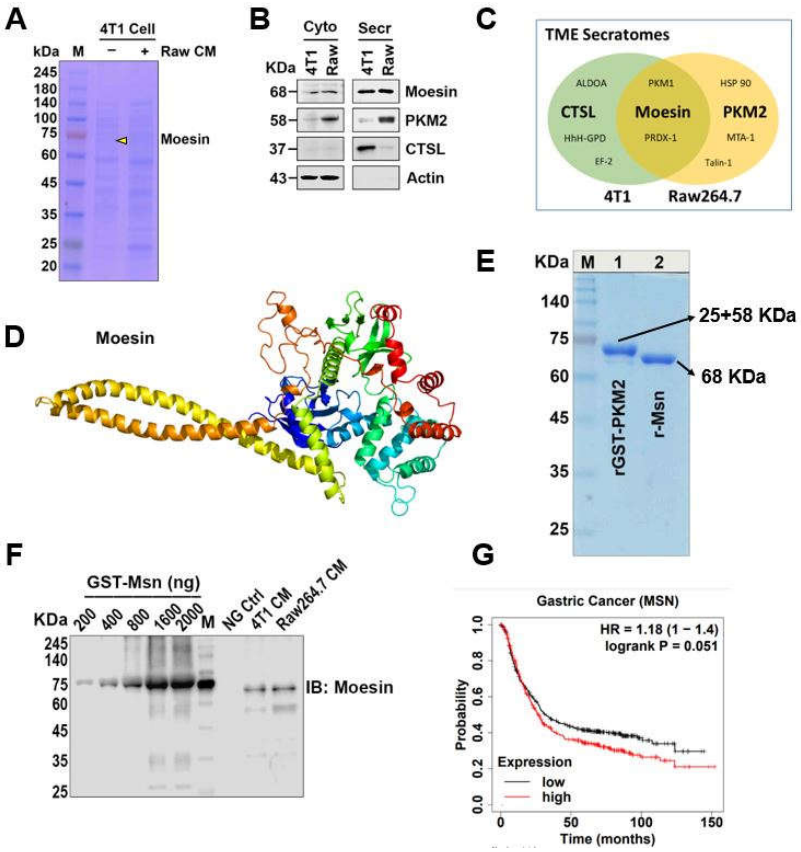

 doi:10.20944/preprints202602.1249.v1

Figure 1. Identification of Msn as a shared secreted protein from 4T1 breast cancer cells and RAW264.7 macrophages. (A) Conditioned media from 4T1 cells alone and from 4T1 cells co-cultured with RAW264.7 macrophages was subjected to Coomassie-blue staining before the mass spectrometry (MALDI-TOF) analysis. Secreted proteins were concentrated using Vivaspin (5 kDa cut-off) and were separated on a 4-15% gradient SDS-PAGE gel. (B) Secreted proteins from cancer cells (4T1) and macrophage cells (Raw264.7) as well as cytosolic proteins were separated by SDS-PAGE and confirmed by western blotting, with 20 μg of protein loaded per well. (C) Venn diagram was generated using specific and common secreted proteins of 4T1 and Raw264.7 cells after mass spectrometry analysis. (D) Crystallographic Msn 3D structure was obtained from the protein data bank (PDB). (E) Validation of rMsn after thrombin cleavage, as a positive control 1 μg of GST-PKM2 was used. Representative Coomassie Blue staining is shown. (F) The amount of Msn secretion from an identical number of 4T1 and Raw264.7 cells. CM was equalized and 15 μg of the protein per lane as well as negative control (NG Ctrl) were loaded for western blot analysis. As a positive control, rGST-Msn was loaded at concentrations of 200 ng to 2000 ng/well and subjected to immunoblotting with the Moesin antibody. (G) Survival probability of gastric cancer patients of the low or high Msn mRNA level was presented by Kaplan-Meier plotter (p=0.051). Representative images were shown.

2.2. Intracellular Signaling Through Extracellular Msn and Cell Physiology in TME

To evaluate the functional role of extracellular Msn in the tumor microenvironment, following our previous study [5], the co-culture system produced a significant level of ROS as well as enhanced cell migration. Consequently, RAW264.7 cells were treated with conditioned media (CM) from 4T1 cells, which resulted in a significant increase in superoxide production and cell migration. Neutralization of Msn with a specific antibody markedly suppressed CM-induced superoxide generation (Figure 2A) and migration (Figure 2B) in macrophage cells, indicating that extracellular Msn is a key mediator of oxidative signaling and migratory responses in macrophages.

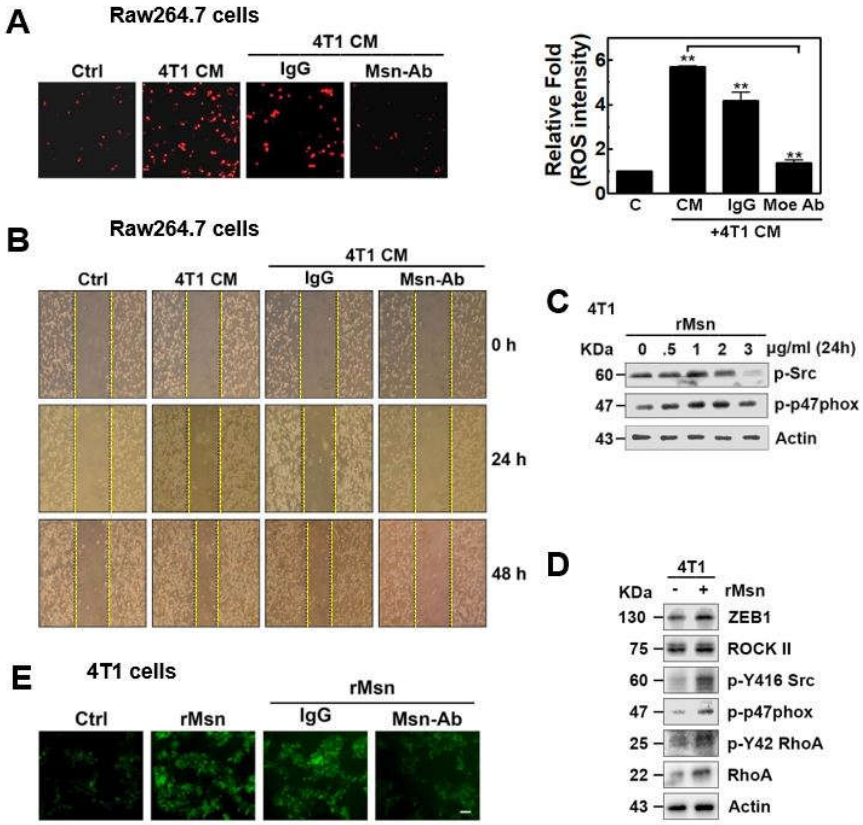

Figure 2. Intracellular signaling through extracellular Msn and cell physiology in TME. (A, B) Raw264.7 cells were cultured with serum-depleted medium for 7 h then pretreated with 2 μg/mL Msn antibody and a control

 doi:10.20944/preprints202602.1249.v1

IgG for 1 h, then incubated with 4T1 CM for 24 h. (A) superoxide production was visualized by 10 μM DHE and (B) after scratching, cells were subjected to the indicated treatments and the migration index was measured at various time points at 0, 24 and 48 h. (C, D) 4T1 cells were treated with rMsn in a concentration-dependent manner (C) and 1 μg/mL (D) for 24 h, then harvested cell lysates were subjected to western blot analysis. (E) Similar to Figure 2A, 4T1 cells were pretreated with 1 μg/mL Msn antibody and a control IgG for 1 h, then incubated with 1 μg/mL rMsn for 24 h, superoxide production was visualized by 5 μM DCF-DA. Data are representative of three independent biological replicates.

Then, we aimed to identify downstream targets of extracellular Msn, whether involved in epithelial–mesenchymal transition (EMT), RhoA/ROCK signaling, and ROS-associated feedback regulation in cancer cells. In addition, our previous study showed that ROS generation in stimulated cancer cells was shown to involve Src-dependent Tyr42 phosphorylation of RhoA [33], and ROCK-mediated phosphorylation of the NOX2 subunit p47phox at Ser345 [34]. Accordingly, rMsn was applied to 4T1 cancer cells in a concentration-dependent manner. Western blot analysis demonstrated that treatment with 1 μg/mL rMsn optimally increased phosphorylation of Src at Tyr416 and p47^phox at Ser345 (Figure 2C). Consistent with these findings, treatment of 4T1 cells with rMsn increased total RhoA protein levels and induced phosphorylation of RhoA at Tyr42. rMsn treatment also elevated ROCK2 expression and enhanced phosphorylation of Src at Tyr416 and p47phox at Ser345, key regulators of superoxide generation in cancer cells. In parallel, expression of ZEB1, a transcriptional repressor of E-cadherin and a central regulator of EMT, was increased following rMsn treatment (Figure 2D). Western blot analyses showed coordinated changes in EMT- and ROS-associated signaling proteins following rMsn treatment, consistent with activation of the RhoA–ROCK pathway and enhanced superoxide generation in cancer cells. In this study, rMsn was expressed in E. coli, potential endotoxin-like effects, such as LPS contamination, were considered. Treatment of 4T1 cancer cells with rMsn significantly increased superoxide generation, while co-treatment with a Msn-specific anti-body markedly reduced this response (Figure 2E). These data indicate that secreted Msn is critically associated with increased ROS production in the TME and correlates with EMT-related migratory signaling.

2.3. Extracellular Msn (exMsn) Interacts with Extracellular PKM2 (exPKM2)

It is well known that, Msn is a member of the ERM protein family and interacts with ezrin and radixin to regulate cytoskeletal dynamics. Phosphorylation at a conserved threonine residue induces a conformational change that exposes ERM binding sites, enabling interactions with down-stream signaling partners. CD44 cross-linking has been shown to increase Msn phosphorylation at Thr558, thereby promoting breast cancer cell migration and invasion [35]. Based on this, we hypothesized whether Msn interacts with other proteins within the tumor microenvironment. Because a potential interaction between PKM2 and Msn has not been previously reported, and given our prior focus on secreted PKM2, we performed co-immunoprecipitation assays. Immunoprecipitation using antibodies against PKM2 or Msn revealed a physical interaction between the two proteins, as detected by western blot analysis (Figure 3A). Interestingly, STRING database analysis indicated that Msn is predicted to interact with multiple proteins, including RhoA, ROCK1/2, CD93, and ICAM1, as illustrated in Figure 3B. This study aimed to evaluate the extracellular interaction between Msn and PKM2 in the tumor microenvironment. Therefore, collected conditioned media (CM) were concentrated, and subjected to co-immunoprecipitation analysis. Msn–PKM2 interaction was detected under extracellular conditions, with increased binding observed during co-culture (Figure 3C and D). In contrast, simple mixing of CM from both cell types resulted in reduced detectable Msn-PKM2 interaction, suggesting differential stability or interaction dynamics. Collectively, these results identify PKM2 as a binding partner of Msn in the tumor microenvironment.

 doi:10.20944/preprints202602.1249.v1

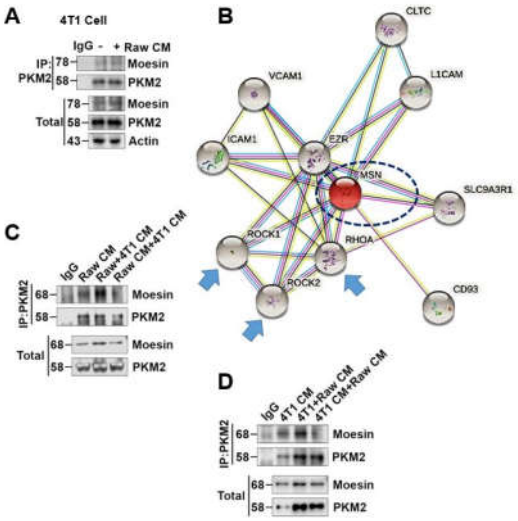

Figure 3. Extracellular Msn (exMsn) interacts with extracellular PKM2 (exPKM2). (A) 4T1 cells were subjected to treated with Raw264.7 CM, then harvested cell lysates underwent co-immunoprecipitation with specific antibodies. Msn and PKM2 interactions were detected by western blot analysis. (B) Protein–protein interaction network analysis of Msn, partner protein interactome generated by STRING with a confidence level of 0.4. (C, D) Representative co-IP using concentrated conditioned media as well as the co-culture system from Raw264.7 cells (C) and 4T1 cells (D).

2.4. exMsn Can Be Phosphorylated by exPKM2 in the Presence of PEP

To further investigate how PKM2 interacts with Msn, we employed an in vitro assay. The 4T1 cells were treated with PEP, a substrate of PKM2, rGST-PKM2 or their combination. After collecting the CM from the cells, equal amounts of CM were probed with a pan-phospho-Ser/Thr and Tyr antibody. Western blot analysis revealed that a number of unidentified proteins were phosphorylated using p-Ser/Thr antibody, while p-Tyr was unable to detect (Figure 4A; upper panel, Figure S2a). The excised bands were analyzed by PMF MALDI-TOF and revealed that Msn and HSP90β were phosphorylated (Figure 4A; bottom panel). For further confirmation, we employed an in vitro kinase assay and found that Msn was phosphorylated by PKM2 in the presence of PEP (Figure 4B, Figure S2b). Then the in vitro kinase sample SDS-PAGE bands were excised and further analyze and revealed that three residues of Msn were phosphorylated, and namely Thr235, Ser243 and Thr413 (Figure 4C; Figure S2c,d).

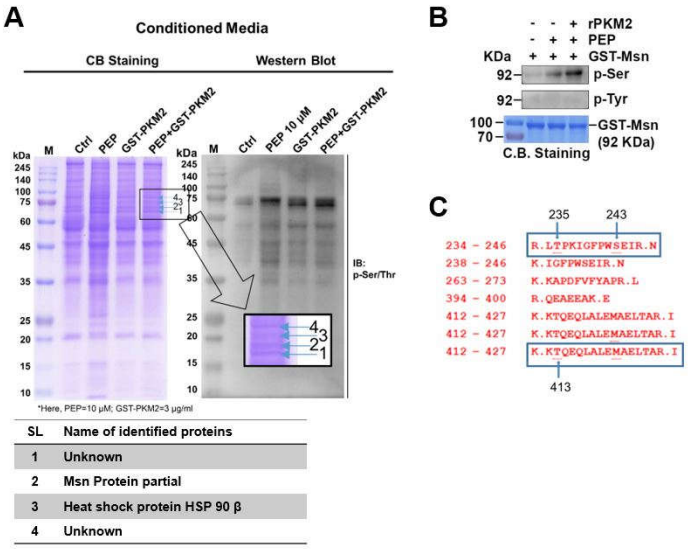

 doi:10.20944/preprints202602.1249.v1

Figure 4. exMsn can be phosphorylated by exPKM2 in a PEP-dependent manner. (A) 4T1 cells were cultured in serum-depleted medium for 8 h and treated with 50 μM PEP, GST-PKM2 40 nM or 3.2 μg/mL alone and in combination then incubated for 24 h. The collected CM from cells was concentrated and subjected to SDS-PAGE, documented by Coomassie Blue (CB) staining and immunoblotting with pan-p-Ser/Thr antibody. Four excised bands were analyzed by MALDI-TOF. (B) Phosphorylation of Msn was confirmed by in vitro kinase assay, representative western blot and CB staining are shown. (C) In vitro kinase samples were analyzed by PMF MALDI-TOF to identify phosphorylation sites, T235, S243 and T413 residues of Msn were phosphorylated.

2.5. N-Terminal Extended α-Helical Globular Domain of Msn Was Phosphorylated by exPKM2

To investigate the specific phosphorylation residues of Msn protein, it is well known that ERM proteins contain three domains. The B41 domain of human Msn known as plasma mem-brane-binding domain. The FERM C-terminal pH like domain, which is also called cytoskeletal-associated domain. Lastly, the ERM molecules contain 3 sub-domains, an N-terminal globular domain; an extended α-helical domain; and a charged C-terminal domain (Figure S3a). To evaluate the true phosphorylation site of Msn, three mutant primers were prepared as a dephospho-mimetic forms (Table 1). Using the wild-type GST-Msn plasmid construct, Thr235 was changed to Alanine (T235A), Ser243 was changed to Cysteine (S243C), and Thr413 was changed to Ala-nine (T413A) (Figure 5A; Figure S3b). Then WT and mutant forms of Msn protein were expressed in E. coli and purified with a GST-tag. The released fusion protein from the beads were subjected to Coomasie-Blue staining after running on an SDS-PAGE gel to confirm the purity (Figure 5B; Figure S3c). Released Msn WT and mutant proteins were subjected to in vitro kinase assay and then western blot analysis by p-Ser/Thr antibody failed to detect the Thr413 residue of Msn (Figure 5C). These results suggest that phosphoenol pyruvate (PEP)-dependent PKM2 phosphorylates the N-terminal extended α-helical globular domain of Msn at Thr413 residue (Figure 5D, Figure S3d). To assess the biological consequence of PKM2–Msn signaling, down-stream epithelial–mesenchymal transition (EMT) markers were analyzed. Treatment with rPKM2 and PEP in the presence of rMsn increased the expression of the mesenchymal transcription factor ZEB1 while reducing the epithelial marker E-cadherin. These effects were attenuated when PKM2 activity or Msn availability was limited, indicating that PKM2-driven phosphorylation of Msn contributes to EMT-associated molecular changes. These results identify Msn as a direct PKM2 substrate in the TME, with Thr235, Ser243, and especially Thr413 phosphorylation driving EMT-associated signaling and revealing a non-metabolic PKM2–Msn axis involved in tumor progression and cellular plasticity.

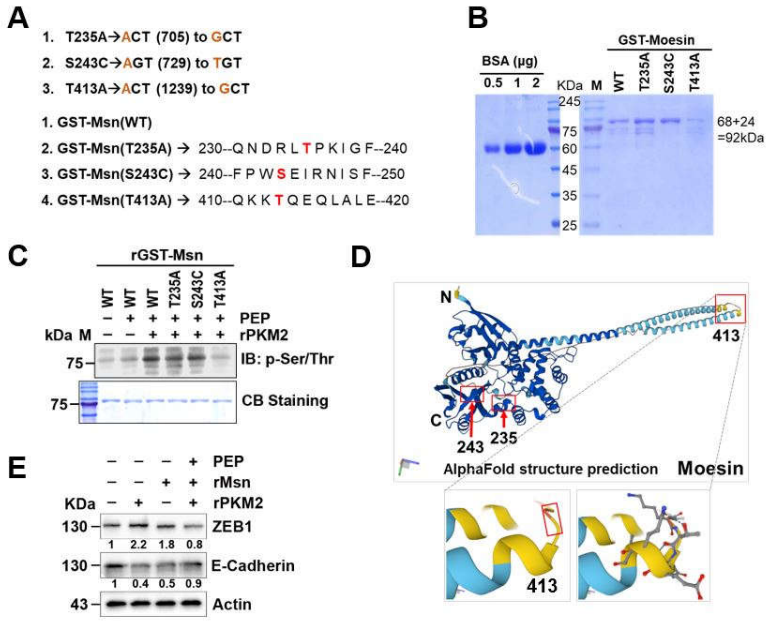

 doi:10.20944/preprints202602.1249.v1

Figure 5. N-terminal extended α-helical globular domain of Msn was phosphorylated by exPKM2. (A) Dephospho-mimetic forms of GST-Msn site-directed mutagenesis primer designs are shown according to the amino acid sequence. (B) GST-Msn WT and mutant protein induction and purification, representative CB staining with BSA used as a positive control. (C) In vitro kinase assay was performed using the released form of rGST-Msn WT and mutant forms with rPKM2 and PEP. Representative western blot images of p-Ser/Thr antibody and CB staining are shown. (D) N-terminal extended α-helical globular domain of Msn at the Thr413 residue was phosphorylated by exPKM2, 3D structure of Msn obtained from the PDB database. (E) Immunoblot analysis of epithelial–mesenchymal transition (EMT) markers following treatment with rMsn, rPKM2, and PEP. Expression levels of ZEB1 and E-cadherin are shown, with actin as a loading control. Relative band intensities are indicated below each lane.

Table 1

SL	Identity	Primer sequence(5′ to 3′)
1	MSN- T235A_F	GAATGACAGACTAGCTCCCAAGATAG
2	MSN- T235A_R	CTATCTTGGGAGCTAGTCTGTCATTC
3	MSN- T243C_F	GGCTTCCCCTGGAGTGAAATCAGGAACATC
4	MSN- T243C_R	GGCTTCCCCTGGTCTGAAATCAGGAACATC
5	MSN- T413A_F	CAGAAAAAGGCTCAGGAACAG
6	MSN- T413A_R	CTGTTCCTGAGCCTTTTTCTG

[1] Primer pairs were used for site-directed mutagenesis.

3. Discussion

Conventionally, intracellular moesin (Msn) functions as an interacting scaffold protein that regulates actin cytoskeleton dynamics and cell motility [36,37]. However, when secreted into the TME, exMsn appears to acquire distinct “moonlighting” functions. Previous studies have shown that intracellular and extracellular Msn exert different functional outcomes in breast cancer cells, including differential regulation of Src activity and β-catenin nu-clear translocation [21]. Moreover, elevated Msn expression promotes epithelial–mesenchymal transition (EMT) by modulating adhesion and contractile components, thereby driving actin filament reorganization and EMT-associated transcriptional programs [38].

In the present study, exMsn was found to activate the RhoA/ROCK2 signaling pathway, accompanied by increased phosphorylation of Src at Tyr416, RhoA at Tyr42, and p47phox at Ser345. These findings indicate the presence of a positive feedforward loop that promotes superoxide generation, as superoxide in turn activates Src Notably, intracellular Msn did not markedly affect RhoA activity, underscoring the context-dependent functions of Msn. This aligns with the known reciprocal regulation between Rho GTPases and ERM proteins [7]. Src-mediated phosphorylation of RhoA and ROCK2-mediated phosphorylation of p47phox likely drive ROS-dependent downstream signaling [34,39]. These intracellular signaling events are known to regulate EMT-associated gene expression, including vimentin and ZEB1 [5,33] Although a previous study reported that exMsn interacts with CD44 and fibronectin (FN1) to suppress cell viability and tumorigenic gene expression, such as Runx2, Snail, and MMP9 [40], our findings demonstrate that exMsn increases ZEB1 levels, a transcriptional repressor of E-cadherin (Figure 2D and 5E), suggesting context- and cell type–specific effects of exMsn in tumor progression.

In our previous study, exPKM2 was identified as a macrophage-derived paracrine signaling molecule that promotes cancer cell migration and invasion. Interestingly, treatment with rPKM2 in the presence of its substrate PEP resulted in a marked reduction of EMT marker expression, accompanied by suppressed cell migration and invasion, with the exception of increased E-cadherin levels [5]. These findings suggest that the functional outcome of exPKM2 signaling in the TME may be modulated by its enzymatic state and extracellular substrate availability. To explore potential reciprocal regulatory mechanisms, we examined whether exPKM2 could directly modify exMsn. Our data demonstrate that, in the presence of PEP, exPKM2 phosphorylates exMsn at Thr413 within the

 doi:10.20944/preprints202602.1249.v1

N-terminal extended α-helical globular domain (Figure 5C). Although the functional consequences of Thr413 phosphorylation remain to be fully elucidated, this modification may alter exMsn stability, conformation, or interaction with extracellular binding partners in the TME. Notably, threonine phosphorylation is a well-established activation mechanism for ERM family proteins, with analogous sites reported in ezrin (T567), radixin (T564), and moesin (T558) that expose functional interaction domains [13,14]. The pronounced reduction in phosphorylation observed in the T413A mutant further identifies this residue as a critical regulatory site. Collectively, these findings implicate exMsn as a functionally relevant extracellular substrate of exPKM2 and suggest that PKM2-mediated phosphorylation of exMsn may act as a molecular switch regulating EMT-associated signaling. Targeting the exPKM2–exMsn interaction or Thr413 phosphorylation therefore represents a potential therapeutic strategy to limit invasive tumor behavior.

4. Materials and Methods

4.1. Cell Culture

RAW264.7 (murine macrophage) and 4T1 (mouse breast cancer) cell lines were cultured in Dulbecco's Modified Eagle Medium (DMEM; Cat. No. LM 001-05) supplemented with 5% heat-inactivated fetal bovine serum (FBS) and 1% penicillin–streptomycin (100 U/mL penicillin and 100 µg/mL streptomycin). Cells were maintained at 37 °C in a humidified incubator containing 5% CO_2 and 95% air.

4.2. Preparation of Conditioned Media (CM)

An equal number of 4T1 and RAW264.7 cells were seeded in 100-mm culture dishes at high density (6.6×10^6 cells per dish) and allowed to attach for 6 h or grown to approximately 80% confluence in DMEM supplemented with 5% FBS. Cells were then washed three times with sterile 1× PBS, and the medium was replaced with serum-depleted, phenol-red–free DMEM (Cat. No. 21063-029). Cells were incubated for 24–36 h to generate conditioned media (CM).

The CM were collected and centrifuged at maximum speed to remove floating cells and cellular debris. Supernatants were subsequently concentrated using Centricon centrifugal filter units with a 10-kDa molecular weight cutoff (Sigma-Aldrich, Cat. No. UFC9010, USA). Serum-depleted medium incubated without cells was processed in parallel as a negative control. Protein concentrations of the concentrated CM were quantified using a BCA assay. Finally, CM aliquots were stored at −80 °C to avoid repeated freeze–thaw cycles.

4.3. Recombinant Msn Preparation

The human moesin (hMsn) coding sequence (CDS) was cloned into the bacterial expression vector pGEX-4T-1 (Addgene plasmid #11637), which encodes an N-terminal GST tag with a thrombin cleavage site. GST–MSN fusion protein expression was induced in Escherichia coli BL21 cells by the addition of 0.3 mM isopropyl β-D-1-thiogalactopyranoside (IPTG) and incubation for 4–5 h at 28 °C with shaking at 80 rpm.

Following induction, bacterial cells were lysed in GST fusion protein lysis buffer (20 mM HEPES, pH 7.4, 150 mM NaCl, 5 mM $MgCl_2$, and 1% Triton X-100) supplemented with protease and phosphatase inhibitor cocktails. Clarified lysates containing GST–MSN were incubated with glutathione (GSH)–Sepharose 4B beads for affinity purification. Beads were washed seven times with wash buffer (20 mM HEPES, 150 mM NaCl, 1 mM $MgCl_2$, supplemented with inhibitors) to ensure protein purity.

Bound GST–MSN was cleaved on-bead using thrombin according to the manufacturer's instructions (Sigma-Aldrich, Cat. No. RECOMT-1KT, USA) to remove the GST tag. The purity of recombinant MSN protein was assessed at each purification step by SDS-PAGE followed by

 doi:10.20944/preprints202602.1249.v1

Coomassie Brilliant Blue staining, with bovine serum albumin (BSA) used as a reference standard. Purified rMsn protein was aliquoted and stored at −80 °C until further use.

4.4. Cell Migration by Wound Healing Assay

Cells were seeded into 12-well plates and cultured to approximately 80% confluence. Cells were then serum-starved for 8 h, after which a uniform scratch was generated across the center of each well using a sterile 1-mL pipette tip held at a 60° angle. Floating cells and debris were removed by washing with serum-depleted medium. Cells were subsequently treated with the indicated stimulants, including conditioned medium (CM), rMsn, or antibody in combination with rMsn or CM.

Cell migration at the wound edge was monitored by capturing images using an inverted light microscope (Axiovert 200, Zeiss). Wound areas were quantified using ImageJ software, and relative wound closure was calculated as previously described. Graphical representations were generated using GraphPad Prism 8.

4.5. In Vitro Kinase Assay

Purified recombinant moesin–wild type (rMsn-WT; 0.1 μg) was incubated with recombinant PKM2 (rPKM2; 0.1 μg) and phosphoenolpyruvate (PEP; 100 μM) in kinase assay buffer containing 20 mM HEPES (pH 7.5), 2 mM β-glycerophosphate, 20 mM $MgCl_2$, and 20 mM ATP for 45 min at 30 °C. Phosphorylation of serine/threonine residues was detected by Western blotting using anti–phospho-Ser/Thr antibodies.

Similarly, purified recombinant GST-tagged moesin (rGST-Msn) wild type and mutant forms (rGST-Msn T235A, rGST-Msn S243C, and rGST-Msn T413A) were eluted from glutathione beads using 5 mM reduced glutathione (GSH). After normalization of protein concentrations, in vitro kinase assays were performed by incubating rGST-Msn wild type or mutant proteins (1 μg) with rPKM2 (0.5 μg) and 100 μM PEP in kinase assay buffer under the same conditions.

4.6. Site-Directed Mutagenesis

The pGEX-4T1–MSN (1–577) plasmid was obtained from Addgene (plasmid #11637). Site-directed mutagenesis was performed to generate MSN point mutants (T235A, S243C, and T413A) using a commercial mutagenesis kit (Intron Biotechnology, Sungnam, Korea; Cat. No. 15071), according to the manufacturer's instructions. All mutant constructs were expressed in Escherichia coli BL21 cells using the pGEX-4T1 bacterial expression vector. Primer sequences used for mutagenesis are listed in Tables 1.

4.7. Western Blotting

Briefly, cells were harvested and lysed using RIPA buffer (150 mM NaCl, 20 mM Tris-HCl, pH 7.4, 1 mM EDTA and 1% Nonidet P-40 (NP-40), containing 10 μL/mL of 100X protease inhibitor cocktail (Abbkine, #BMP1001) and 1 mM each of phosphatase inhibitors (NaF and Na2VO3) and then sonicated and vortexed 5-6 times with intervals. The lysate was then centrifuged at 15,800 x g for 15 min at 4 °C. For western blot analysis, the protein concentration in the collected supernatant was determined using a BCA assay kit (PierceTM, #23225, Thermo Scientific, USA). Equal amounts of protein or concentrated CM were then boiled in a sample buffer at 100 °C, and 20 μg/well-loaded proteins were separated by SDS-PAGE in a running tank with 1X running buffer (3gm Tris, 1gm SDS and 14.4gm Glycine) for 2 h at 90 V. Then, separated proteins were transferred to polyvinylidene difluoride (PVDF) membrane (Immobilon®-P TM, #IPVH00010, Millipore) using a transfer tank with 1X transfer buffer at 190 mAmp according to protein size (min/kDa). The membrane was blocked either with 5% skim milk solution or 1X EZ block solution (EZBlockChemi, #AE1475, ATTO, Japan) for 40 min at RT. The membranes were incubated with primary antibodies (dilution mentioned in the Table) overnight at 4 °C and then bound to the HRP-conjugated secondary antibodies (1:5000 or 4000)

 doi:10.20944/preprints202602.1249.v1

for 2 h at RT. Between each step, membranes were washed 3 times by 1X TBST on an 80 RPM shaker. Then a gel documentation system was used to identify the protein band on the membrane after it had been treated with enhanced chemiluminescence (ECL) reagents from Amersham in Uppsala, Sweden. The intensity of the protein bands on the membrane was quantified using ImageJ, a software tool developed by the U.S. National Institutes of Health in Bethesda, USA.

4.8. Immunoprecipitation

Collected cell culture supernatants were concentrated using centrifugal filter units with a 5-kDa molecular weight cutoff. Equal amounts of conditioned medium protein (40 μg) were subjected to a pre-clearing step by incubation with Protein A/G agarose beads for 2 h at 4 °C. The pre-cleared conditioned media were then incubated with anti-PKM2 antibody overnight at 4 °C with gentle rotation (5 rpm) to allow antibody–antigen binding. Protein A/G–conjugated beads were subsequently added and incubated for an additional 4 h to precipitate immune complexes. Beads were washed twice with IP wash buffer and boiled in 2× SDS sample buffer for 10 min. Protein–protein interactions were analyzed by Western blotting.

4.9. Superoxide Measurement Assay

Intracellular superoxide and reactive oxygen species (ROS) levels were measured using dihydroethidium (DHE; Invitrogen, Cat. No. D23107) and 2′,7′-dichlorofluorescein (DCF; Abcam, Cat. No. ab113851) assays to detect red and green fluorescence, respectively. Briefly, 2×10^5 cells were stimulated with the indicated treatments, including conditioned medium (CM), rMsn, or antibody in combination with rMSN or CM, in serum-free medium. Following treatment, cells were washed twice with 1× PBS and fixed with 4% paraformaldehyde at room temperature for 15 min in the dark. Cells were then incubated with either 10 μM DHE or 5 μM DCF for 15 min at room temperature, protected from light, and washed twice with 1× PBS. Fluorescence images were acquired using a fluorescence microscope (Axiovert 200; Carl Zeiss, Göttingen, Germany) with excitation wavelengths of 540–552 nm and emission collected above 590 nm. Image acquisition and processing were performed using IPLab software (version 3.65α).

4.10. Protein Identification by Mass Spectrometry (PMF-MALDI-TOF)

The proteins in CM secreted macrophage and cancer cell lines were identified by mass spectrophotometry. The proteins in CM were separated by SDS-PAGE and visualized by Coomassie-Blue staining (R-250, #CVC006), and then the protein bands of interest were excised from the gel using sterile surgical blade. Those excised bands were sent to the GENOMINE (S-SIMS, Pohang, Korea) company for identification using Peptide Mass Fingerprinting (PMF). In this method, the protein spots were digested with trypsin, and the resulting peptides were mixed with α-cyano-4-hydroxycinnamic acid in 50% acetonitrile/0.1% TFA. The samples were then subjected to MALDI-TOF analysis using a Microflex LRF 20 instrument from Bruker Daltonics, following the protocol described by Fernandez et al. During MALDI-TOF analysis, spectra were collected by acquiring 300 shots per spectrum over the mass-to-charge ratio (m/z) range of 700-4000. The spectra were calibrated using two-point internal calibration with Trypsin auto-digestion peaks (m/z 842.5099, 2211.1046). Flex Analysis 3.0 software was used to generate the peak list with the following threshold parameters: a minimum resolution of monoisotopic mass set to 500 and a signal-to-noise ratio of 6. Protein identification was performed using the MASCOT search program developed by The Matrixscience (http://www.matrixscience.com/). The database search was conducted with the following parameters: trypsin as the cleaving enzyme, allowance of a maximum of one missed cleavage, iodoacetamide (Cys) as a complete modification, oxidation (Met) as a partial modification, monoisotopic masses, and a mass tolerance of ±0.2 Da. The identification of proteins by peptide mass fingerprinting was based on probability scoring using PMF acceptance criteria.

4.11. Bioinformatics Analysis

 doi:10.20944/preprints202602.1249.v1

To generate the survival graph, Kaplan-Meier Plotter (KM Plotter) website (https://kmplot.com/analysis/index.php?p=service&cancer=gastric) was used. In case of stomach cancer, the Msn (#2—600_at) mRNA was selected through 875 patients' information parameters were drawn. Msn crystal structure was obtained from the PDB database. STRING (search tool for the retrieval of interacting genes/proteins) is a web-based server that was used for the study of the protein–protein interaction of Msn (Msn). For the study of Msn interacting partners, a high confidence score of 0.400 was used to generate the protein networks. Designing primers for site-directed mutagenesis, NCBI reference sequence of Homo sapiens Msn (MSN), mRNA (NM_002444.3) were used. Protein Homology/analogY Recognition Engine V 2.0 (Phyre2) was used to generate the alpha fold protein structure.

4.12. Statistical Analysis

The results are expressed as the mean ± standard deviation (SD). All experiments were performed at least in triplicate to ensure reproducibility and intra-assay samples were analyzed in duplicate or triplicate. Statistical analysis was performed using a two-tailed, unpaired Student's t-test to compare differences between the two groups. For multiple group comparisons, one-way or two-way ANOVA followed by the GraphPad Prism program (Version-8, GraphPad Software, San Diego, USA) was employed. Statistical significance was considered when the P values were below the specified limit (*P < 0.05, **P < 0.01, ***P < 0.001).

5. Conclusions

Extracellular moesin functions as a context-dependent signaling mediator in the tumor microenvironment by activating the Src/RhoA/ROCK2 axis and promoting EMT-related signaling. Our findings identify exPKM2-mediated phosphorylation of exMsn at Thr413 as a key regulatory event, highlighting the exPKM2–exMsn axis as a potential therapeutic target for limiting tumor invasion and progression.

Supplementary Materials: The following supporting information can be downloaded at the website of this paper posted on Preprints.org, Figure S1: Secreted Msn Phosphorylated by PKM2 Function in the Tumor Micro-Environment.

Author Contributions: Conceptualization, J.B.P.; methodology, A.H.; software, A.H.; validation, J.B.P., and A.H.; formal analysis, A.H.; investigation, A.H.; resources, A.H., O.D. and S.M; data curation, A.H., and O.D.; writing—original draft preparation, A.H.; writing—review and editing, J.B.P., and A.H.; visualization, A.H.; supervision, J.B.P.; project administration, J.B.P.; funding acquisition, J.B.P. All authors have read and agreed to the published version of the manuscript.

Funding: This work was supported by the National Research Foundation of Korea (NRF) of Korea to JBP [RS-2023-00208724; RS-2023-00217013], and "The APC was waved by MDPI".

Institutional Review Board Statement: Not applicable.

Informed Consent Statement: Not applicable for studies not involving humans.

Data Availability Statement: Supporting data will be found in supplementary file, and raw data will provide upon request.

Conflicts of Interest: The authors declare no conflicts of interest.

Abbreviations

The following abbreviations are used in this manuscript:

TME	Tumor Microenviromnment
exMsn	Extracellular Moesin

 doi:10.20944/preprints202602.1249.v1

rMsn	Recombinant Moesin
exPKM2	Extracellular Pyruvate Kinase
CM	conditioned media
EMT	epithelial-mesenchymal transition

References

1. da Cunha, B.R.; Domingos, C.; Stefanini, A.C.B.; Henrique, T.; Polachini, G.M.; Castelo-Branco, P.; Tajara, E.H. Cellular Interactions in the Tumor Microenvironment: The Role of Secretome. *J Cancer* **2019**, *10*, 4574-4587, doi:10.7150/jca.21780.
2. Morimoto, H.; Ito, Y.; Yoden, E.; Horie, M.; Tanaka, N.; Komurasaki, Y.; Yamamoto, R.; Mihara, K.; Minami, K.; Hirato, T. Non-clinical evaluation of JR-051 as a biosimilar to agalsidase beta for the treatment of Fabry disease. *Mol Genet Metab* **2018**, *125*, 153-160, doi:10.1016/j.ymgme.2018.07.009.
3. Winkler, J.K.; Haenssle, H.A.; Enk, A.; Toberer, F. Orange Verrucous Pitted Lesion on Lateral Foot of a 9-year-old Girl: A Quiz. *Acta Derm Venereol* **2020**, *100*, adv00201, doi:10.2340/00015555-3544.
4. Xue, H.; Lu, B.; Lai, M. The cancer secretome: a reservoir of biomarkers. *J Transl Med* **2008**, *6*, 52, doi:10.1186/1479-5876-6-52.
5. Hamza, A.; Cho, J.Y.; Cap, K.C.; Hossain, A.J.; Kim, J.G.; Park, J.B. Extracellular pyruvate kinase M2 induces cell migration through p-Tyr42 RhoA-mediated superoxide generation and epithelial-mesenchymal transition. *Free Radic Biol Med* **2023**, *208*, 614-629, doi:10.1016/j.freeradbiomed.2023.09.016.
6. Kessenbrock, K.; Plaks, V.; Werb, Z. Matrix metalloproteinases: regulators of the tumor microenvironment. *Cell* **2010**, *141*, 52-67, doi:10.1016/j.cell.2010.03.015.
7. Fehon, R.G.; McClatchey, A.I.; Bretscher, A. Organizing the cell cortex: the role of ERM proteins. *Nat Rev Mol Cell Biol* **2010**, *11*, 276-287, doi:10.1038/nrm2866.
8. Eustace, B.K.; Sakurai, T.; Stewart, J.K.; Yimlamai, D.; Unger, C.; Zehetmeier, C.; Lain, B.; Torella, C.; Henning, S.W.; Beste, G.; et al. Functional proteomic screens reveal an essential extracellular role for hsp90 alpha in cancer cell invasiveness. *Nat Cell Biol* **2004**, *6*, 507-514, doi:10.1038/ncb1131.
9. Lankes, W.T.; Furthmayr, H. Moesin: a member of the protein 4.1-talin-ezrin family of proteins. *Proc Natl Acad Sci U S A* **1991**, *88*, 8297-8301, doi:10.1073/pnas.88.19.8297.
10. Chen, Q.Y.; Xu, W.; Jiao, D.M.; Wu, L.J.; Song, J.; Yan, J.; Shi, J.G. Silence of ezrin modifies migration and actin cytoskeleton rearrangements and enhances chemosensitivity of lung cancer cells in vitro. *Mol Cell Biochem* **2013**, *377*, 207-218, doi:10.1007/s11010-013-1586-x.
11. Kunda, P.; Pelling, A.E.; Liu, T.; Baum, B. Moesin controls cortical rigidity, cell rounding, and spindle morphogenesis during mitosis. *Curr Biol* **2008**, *18*, 91-101, doi:10.1016/j.cub.2007.12.051.
12. Neisch, A.L.; Fehon, R.G. Ezrin, Radixin and Moesin: key regulators of membrane-cortex interactions and signaling. *Curr Opin Cell Biol* **2011**, *23*, 377-382, doi:10.1016/j.ceb.2011.04.011.
13. Adyshev, D.M.; Dudek, S.M.; Moldobaeva, N.; Kim, K.M.; Ma, S.F.; Kasa, A.; Garcia, J.G.; Verin, A.D. Ezrin/radixin/moesin proteins differentially regulate endothelial hyperpermeability after thrombin. *Am J Physiol Lung Cell Mol Physiol* **2013**, *305*, L240-255, doi:10.1152/ajplung.00355.2012.
14. Wei, X.; He, S.; Wang, Z.; Wu, J.; Zhang, J.; Cheng, Y.; Yang, J.; Xu, X.; Chen, Z.; Ye, J.; et al. Fibroblast growth factor 1attenuates 6-hydroxydopamine-induced neurotoxicity: an in vitro and in vivo investigation in experimental models of parkinson's disease. *Am J Transl Res* **2014**, *6*, 664-677.
15. Wang, Q.; Fan, A.; Yuan, Y.; Chen, L.; Guo, X.; Huang, X.; Huang, Q. Role of Moesin in Advanced Glycation End Products-Induced Angiogenesis of Human Umbilical Vein Endothelial Cells. *Sci Rep* **2016**, *6*, 22749, doi:10.1038/srep22749.
16. Li, Q.; Liu, H.; Du, J.; Chen, B.; Li, Q.; Guo, X.; Huang, X.; Huang, Q. Advanced glycation end products induce moesin phosphorylation in murine brain endothelium. *Brain Res* **2011**, *1373*, 1-10, doi:10.1016/j.brainres.2010.12.032.
17. Wang, Y.; Kaiser, M.S.; Larson, J.D.; Nasevicius, A.; Clark, K.J.; Wadman, S.A.; Roberg-Perez, S.E.; Ekker, S.C.; Hackett, P.B.; McGrail, M.; et al. Moesin1 and Ve-cadherin are required in endothelial cells during in vivo tubulogenesis. *Development* **2010**, *137*, 3119-3128, doi:10.1242/dev.048785.

 doi:10.20944/preprints202602.1249.v1

18. Li, Y.Q.; Zheng, Z.; Liu, Q.X.; Lu, X.; Zhou, D.; Zhang, J.; Zheng, H.; Dai, J.G. Moesin as a prognostic indicator of lung adenocarcinoma improves prognosis by enhancing immune lymphocyte infiltration. *World J Surg Oncol* **2021**, *19*, 109, doi:10.1186/s12957-021-02229-y.
19. Siu, L.L. Clinical trials in the elderly--a concept comes of age. *N Engl J Med* **2007**, *356*, 1575-1576, doi:10.1056/NEJMe078023.
20. Kwon, O.K.; Lee, W.; Kim, S.J.; Lee, Y.M.; Lee, J.Y.; Kim, J.Y.; Bae, J.S.; Lee, S. In-depth proteomics approach of secretome to identify novel biomarker for sepsis in LPS-stimulated endothelial cells. *Electrophoresis* **2015**, *36*, 2851-2858, doi:10.1002/elps.201500198.
21. Ahandoust, S.; Li, K.; Sun, X.; Li, B.Y.; Yokota, H.; Na, S. Intracellular and extracellular moesins differentially regulate Src activity and beta-catenin translocation to the nucleus in breast cancer cells. *Biochem Biophys Res Commun* **2023**, *639*, 62-69, doi:10.1016/j.bbrc.2022.11.075.
22. Gao, X.; Wang, H.; Yang, J.J.; Liu, X.; Liu, Z.R. Pyruvate kinase M2 regulates gene transcription by acting as a protein kinase. *Mol Cell* **2012**, *45*, 598-609, doi:10.1016/j.molcel.2012.01.001.
23. Jiang, Y.; Wang, Y.; Wang, T.; Hawke, D.H.; Zheng, Y.; Li, X.; Zhou, Q.; Majumder, S.; Bi, E.; Liu, D.X.; et al. PKM2 phosphorylates MLC2 and regulates cytokinesis of tumour cells. *Nat Commun* **2014**, *5*, 5566, doi:10.1038/ncomms6566.
24. Koppenol, W.H.; Bounds, P.L.; Dang, C.V. Otto Warburg's contributions to current concepts of cancer metabolism. *Nat Rev Cancer* **2011**, *11*, 325-337, doi:10.1038/nrc3038.
25. Yang, W.; Xia, Y.; Ji, H.; Zheng, Y.; Liang, J.; Huang, W.; Gao, X.; Aldape, K.; Lu, Z. Nuclear PKM2 regulates β-catenin transactivation upon EGFR activation. *Nature* **2011**, *480*, 118-122.
26. Wang, C.; Zhang, S.; Liu, J.; Tian, Y.; Ma, B.; Xu, S.; Fu, Y.; Luo, Y. Secreted Pyruvate Kinase M2 Promotes Lung Cancer Metastasis through Activating the Integrin Beta1/FAK Signaling Pathway. *Cell Rep* **2020**, *30*, 1780-1797 e1786, doi:10.1016/j.celrep.2020.01.037.
27. Hou, P.P.; Luo, L.J.; Chen, H.Z.; Chen, Q.T.; Bian, X.L.; Wu, S.F.; Zhou, J.X.; Zhao, W.X.; Liu, J.M.; Wang, X.M.; et al. Ectosomal PKM2 Promotes HCC by Inducing Macrophage Differentiation and Remodeling the Tumor Microenvironment. *Mol Cell* **2020**, *78*, 1192-1206 e1110, doi:10.1016/j.molcel.2020.05.004.
28. Whitesell, L.; Lindquist, S.L. HSP90 and the chaperoning of cancer. *Nat Rev Cancer* **2005**, *5*, 761-772, doi:10.1038/nrc1716.
29. Wang, X.; Song, X.; Zhuo, W.; Fu, Y.; Shi, H.; Liang, Y.; Tong, M.; Chang, G.; Luo, Y. The regulatory mechanism of Hsp90alpha secretion and its function in tumor malignancy. *Proc Natl Acad Sci U S A* **2009**, *106*, 21288-21293, doi:10.1073/pnas.0908151106.
30. Zhang, S.; Wang, C.; Ju, J.; Wang, C. Extracellular Hsp90alpha Supports the ePKM2-GRP78-AKT Axis to Promote Tumor Metastasis. *Front Oncol* **2022**, *12*, 906080, doi:10.3389/fonc.2022.906080.
31. Li, Q.; Nance, M.R.; Kulikauskas, R.; Nyberg, K.; Fehon, R.; Karplus, P.A.; Bretscher, A.; Tesmer, J.J. Self-masking in an intact ERM-merlin protein: an active role for the central alpha-helical domain. *J Mol Biol* **2007**, *365*, 1446-1459, doi:10.1016/j.jmb.2006.10.075.
32. Vilmos, P.; Kristo, I.; Szikora, S.; Jankovics, F.; Lukacsovich, T.; Kari, B.; Erdelyi, M. The actin-binding ERM protein Moesin directly regulates spindle assembly and function during mitosis. *Cell Biol Int* **2016**, *40*, 696-707, doi:10.1002/cbin.10607.
33. Kim, J.G.; Mahmud, S.; Min, J.K.; Lee, Y.B.; Kim, H.; Kang, D.C.; Park, H.S.; Seong, J.; Park, J.B. RhoA GTPase phosphorylated at tyrosine 42 by src kinase binds to beta-catenin and contributes transcriptional regulation of vimentin upon Wnt3A. *Redox Biol* **2021**, *40*, 101842, doi:10.1016/j.redox.2020.101842.
34. Cap, K.C.; Kim, J.G.; Hamza, A.; Park, J.B. P-Tyr42 RhoA GTPase amplifies superoxide formation through p47phox, phosphorylated by ROCK. *Biochem Biophys Res Commun* **2020**, *523*, 972-978, doi:10.1016/j.bbrc.2020.01.001.
35. Hu, S.; Shi, X.; Liu, Y.; He, Y.; Du, Y.; Zhang, G.; Yang, C.; Gao, F. CD44 cross-linking increases malignancy of breast cancer via upregulation of p-Moesin. *Cancer Cell Int* **2020**, *20*, 563, doi:10.1186/s12935-020-01663-4.
36. Sanchez-Sanchez, B.J.; Marcotti, S.; Salvador-Garcia, D.; Diaz-de-la-Loza, M.D.; Burki, M.; Davidson, A.J.; Wood, W.; Stramer, B.M. Moesin integrates cortical and lamellar actin networks during Drosophila macrophage migration. *Nat Commun* **2025**, *16*, 1414, doi:10.1038/s41467-024-55510-5.

 doi:10.20944/preprints202602.1249.v1

37. Barros, F.B.A.; Assao, A.; Garcia, N.G.; Nonogaki, S.; Carvalho, A.L.; Soares, F.A.; Kowalski, L.P.; Oliveira, D.T. Moesin expression by tumor cells is an unfavorable prognostic biomarker for oral cancer. *BMC Cancer* **2018**, *18*, 53, doi:10.1186/s12885-017-3914-0.
38. Haynes, J.; Srivastava, J.; Madson, N.; Wittmann, T.; Barber, D.L. Dynamic actin remodeling during epithelial-mesenchymal transition depends on increased moesin expression. *Mol Biol Cell* **2011**, *22*, 4750-4764, doi:10.1091/mbc.E11-02-0119.
39. Tlili, A.; Pintard, C.; Hurtado-Nedelec, M.; Liu, D.; Marzaioli, V.; Thieblemont, N.; Dang, P.M.; El-Benna, J. ROCK2 interacts with p22phox to phosphorylate p47phox and to control NADPH oxidase activation in human monocytes. *Proc Natl Acad Sci U S A* **2023**, *120*, e2209184120, doi:10.1073/pnas.2209184120.
40. Senbanjo, L.T.; Chellaiah, M.A. CD44: A Multifunctional Cell Surface Adhesion Receptor Is a Regulator of Progression and Metastasis of Cancer Cells. *Front Cell Dev Biol* **2017**, *5*, 18, doi:10.3389/fcell.2017.00018.